American Mineralogist, Volume 90, pages 1177–1185, 2005

Dissakisite-(La) from the Ulten zone peridotite (Italian Eastern Alps): A new end-member of the epidote group

SIMONE TUMIATI,[1,2,*] GASTON GODARD,[2] SILVANA MARTIN,[1] PAOLO NIMIS,[3] VOLKMAR MAIR,[4] AND BERNARD BOYER[5]

[1]Dipartimento di Scienze Chimiche e Ambientali, Università degli Studi dell'Insubria, Via Lucini 3, I-22100 Como, Italy
[2]Laboratoire de Géosciences marines, Institut de Physique du Globe, 4, place Jussieu, F-75252 Paris, France
[3]Dipartimento di Mineralogia e Petrologia, Università degli Studi di Padova, C.so Garibaldi 37, I-35100 Padova, Italy
[4]Ufficio Geologia e Prove Materiali, Provincia Autonoma di Bolzano, Via Val d'Ega 48, I-39053 Cardano (Bolzano), Italy
[5]Université Montpellier II, place Eugène Bataillon, F-34095 Montpellier, France

ABSTRACT

Dissakisite-(La), ideally $CaLaAl_2MgSi_3O_{12}(OH)$, has been found in the Hochwart peridotite, Ulten zone, Italy. The mineral occurs as centimeter-sized black to very dark brown anhedral nodules and smaller grains. Associated minerals are: olivine, spinel, amphiboles, clino- and orthopyroxenes, and minor clinochlore, uraninite, thorite, thorianite, phlogopite, zircon, apatite, calcite, dolomite, pentlandite, and copper sulfides. The streak is gray-greenish and the luster is vitreous. Mohs hardness is 6.5–7; the mineral is brittle with a conchoidal fracture. The cleavage is imperfect on (001). Dissakisite-(La) is monoclinic, space group $P2_1/m$. The unit cell dimensions are $a = 8.9616(7)$, $b = 5.7265(5)$, and $c = 10.2353(9)$ Å, $\beta = 115.193(6)°$, $V = 475.30(7)$ Å^3, $Z = 2$. The strongest X-ray powder diffraction lines are: [d(Å) (I)(hkl)] 2.926(100)(11$\bar{3}$), 2.860(53)(020), 2.553(51)(202), 3.526(49)(21$\bar{1}$), 2.699(44)(120). Electron and ion microprobe analysis of the type sample DISS 5 gave the formula $(Ca_{1.195}Mn_{0.009}Sr_{0.010}Na_{0.002}Th_{0.090}U_{0.003}La_{0.315}Ce_{0.262}Pr_{0.019}Nd_{0.038}Sm_{0.002}Gd_{0.001}Er_{0.001})(Al_{1.816}Mg_{0.622}Fe^{2+}_{0.244}Fe^{3+}_{0.159}Cr_{0.148}Ti_{0.030}Sc_{0.002}V_{0.008}Ga_{0.001}Ni_{0.010}Zn_{0.015})(Si_{2.970}Al_{0.022}P_{0.008})O_{11.991}F_{0.009}(OH)$. The La/(La + Ce) ratio is 0.545(16) in the type analysis and 0.543(18) in an average of 70 analyses of the type sample A4310. Ce ≥ La was not observed in any analysis. $D_{meas} = 3.79(15)$ g/cm^3; $D_{calc} = 3.84$ g/cm^3. Radioactivity is appreciable. The optical properties and Raman spectrometry have also been investigated. The mineral formed by hydration and enrichment in LILE and LREE of a peridotite body, in relation to H*P*-migmatization of the surrounding gneisses during the Variscan orogeny.

INTRODUCTION

Magnesian and Mg-rich Rare Earth Element (REE) epidote minerals (collectively termed "allanite") have been found in different types of metamorphic rocks, such as chromiferous mica-schists (Outokumpu, Finland; Treloar and Charnley 1987), garnet-corundum rocks (Su-Lu, China; Enami and Zang 1988), sulfide ores (Bergslagen, Sweden; Zakrzewski et al. 1992), and talc-chlorite deposits (Trimouns, France; Moëlo et al. 1974; Parseval et al. 1997).

Dissakisite-(Ce), ideally $CaCeMgAl_2Si_3O_{12}(OH)$, and dollaseite-(Ce), ideally $CaCeMg_2AlSi_3O_{11}(OH,F)_2$, are two (REE, Mg)-rich members of the epidote group that have been reported in marbles from high-grade metamorphic terranes (Balchen Mountain, East Antarctica; Grew et al. 1991) and skarns (Östanmossa, Sweden; e.g., Geijer 1927; Aldan Shield, Russia; Khvostova and Bykova 1961). Further details on dissakisite historical background can be found in Gieré and Sorensen (2004).

To date, only one occurrence of dissakisite, i.e., a Cr-rich dissakisite-(Ce), has been reported in a peridotite, namely a garnet peridotite from the Su-Lu ultra-high-pressure metamorphic terrane, China (Yang and Enami 2003). This study is focused on the newly discovered occurrence of (Th, Cr)-bearing cerian dissakisite-(La) in a peridotite body from the Ulten zone (Austroalpine domain, Eastern Alps).

Dissakisite-(La) is named for its A2 site cation content, having La > Ce. The mineral thus represents the Mg-analogue of allanite-(La). It is worth noting that Treloar and Charnley (1987) described a "chromian allanite" in the Cr-rich biotite-bearing schists of Outokumpu, Finland. The analyses of this mineral, actually a dissakisite, as noted also by Grew et al. (1991) and Ercit (2002), gave La/(La + Ce) ratios in the range 0.476–0.514, and, in 3 of 11 analyses, La was in fact more abundant than Ce. Nevertheless, Treloar and Charnley (1987) did not identify dissakisite-(La) as a new mineral species.

The new mineral species dissakisite-(La), based on our samples collected from the Ulten zone, was accepted by the Commission on New Minerals and Mineral Names of the International Mineralogical Association on May 27, 2003. The type material has been deposited in museums. (1) A4310, a thin polished section of a centimeter-sized crystal in peridotite matrix, is deposited at the Muséum National d'Histoire Naturelle de Paris (France) as specimen MNHN 203.133. (2) DISS 5, a single grain analyzed for the official chemical composition, and

* E-mail: simone.tumiati@uninsubria.it

(3) DISS 3, a refined single-crystal (Lavina, Carbonin, Russo and Tumiati, unpublished manuscript), are deposited at the Museo di Mineralogia, Università degli Studi di Padova (Italy), as specimen N.INV.1339.

Occurrence and geological overview

A few large, lucent, black to very dark brown grains and pitch-like nodules up to 2.5 cm (Fig. 1) of an epidote mineral were found in a single block of peridotite at the toe of a gully cutting the northern wall of Mt. Hochwart (Ulten Valley, Eastern Italian Alps; N 46°31'4", E 10°59'55"). From the morphology of the area, it is reasonable to assume that the loose block was derived from a garnet-bearing peridotite body exposed on the north wall of the mountain (cf. Andreatta 1936; Rost und Brenneis 1978; Susini e Martin 1996). This garnet peridotite body has Variscan garnet-clinopyroxene and garnet-whole-rock Sm-Nd ages (330 ± 6 Ma; Tumiati et al. 2003). A kyanite-bearing migmatitic gneiss hosts the peridotite. The contacts between the peridotite and the gneiss are sharp but strongly metasomatized, with development of unusual hybrid rocks (Tumiati and Martin 2003).

The Hochwart peridotite is one of several peridotite bodies hosted by migmatitic gneisses in the Ulten zone (e.g., Obata and Morten 1987; Godard et al. 1996). The Ulten peridotites show transformation of the original protogranular spinel lherzolite into a coarse garnet-spinel lherzolite (Obata and Morten 1987). Peak metamorphic conditions for the garnet stage have been estimated at approximately 2.7 GPa and 850 °C (Nimis and Morten 2000). Abundant pargasite formed in hydrated, deformed, and recrystallized domains during the garnet-facies stage, giving rise to fine-grained garnet-amphibole peridotites (Obata and Morten 1987; Tumiati et al. 2003). These amphibole-bearing peridotites record the effect of extensive crustal metasomatism, as indicated by significant alkalis + Large-Ion Lithophile Element (LILE) enrichment (Morten and Obata 1990; Bondi et al. 1992; Ntaflos et al. 1993; Petrini and Morten 1993; Rampone and Morten 2001; Tumiati et al. 2003). In almost all outcrops the peridotites show the development of retrograde minerals, such as magnesiohornblende and spinel, consistent with a decompressional exhumation path (Martin et al. 1998; Godard and Martin 2000).

Current views on the origin of the Ulten peridotites involve incorporation of portions of a mantle wedge into a subducting crustal slab during the Variscan orogeny (Godard et al. 1996; Nimis and Morten 2000; Tumiati et al. 2003).

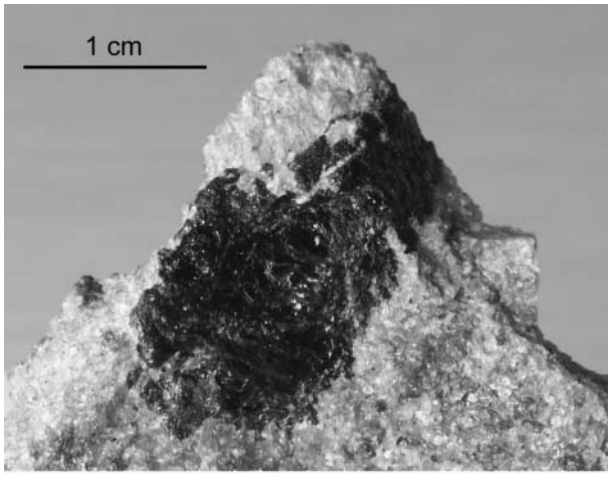

Figure 1. Macrophotograph of dissakisite-(La) from the Ulten zone (Eastern Alps, Italy) in a peridotite matrix.

Petrography and mineralogy of the dissakisite-bearing peridotite

The dissakisite-(La) occurs in a fine-grained spinel-amphibole-bearing peridotite with minor clinopyroxene. The present mineral assemblage was derived by retrogression from a former garnet-bearing peridotite, as proved by the presence of globular spinel-amphibole aggregates, which most likely represent alteration products after garnet. Trails of secondary fluid inclusions and later radial cracks are observed in olivine grains which surround the dissakisite-(La) crystals. The later radial cracks were possibly caused by volume increase of the dissakisite-(La) due to metamictization (cf. Yang and Enami 2003; Lavina, Carbonin, Russo and Tumiati, unpublished manuscript) (Fig. 2).

Olivine (Fo_{91}) is the dominant matrix mineral. It has a porphyroclastic texture, with unaltered crystals from 0.1 mm to over 1 cm in size. Magnesiohornblende (5 vol%; X_{Mg} = 0.93–0.94) occurs in clusters associated with Al-rich spinel. Orthopyroxene (X_{Mg} = 0.90) and clinopyroxene (X_{Mg} = 0.95) are also present as matrix constituents and Cr-rich spinel [Mg/(Mg + Fe) =

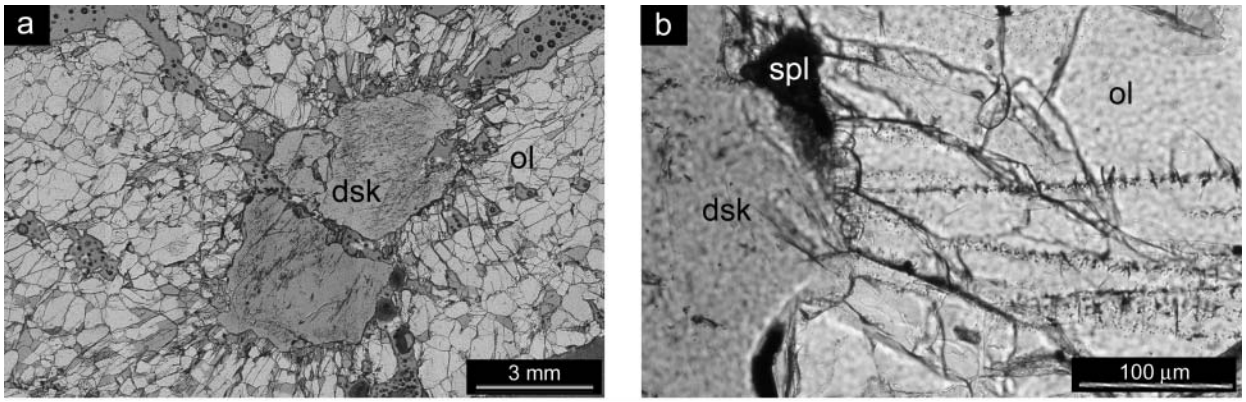

Figure 2. Microphotographs of dissakisite-(La) (dsk), thin section A4310. (**a**) View of the entire sample: radial cracks propagate into the surrounding olivine (ol); (**b**) fluid inclusion trails produced by healing of microfractures (plane-polarized light).

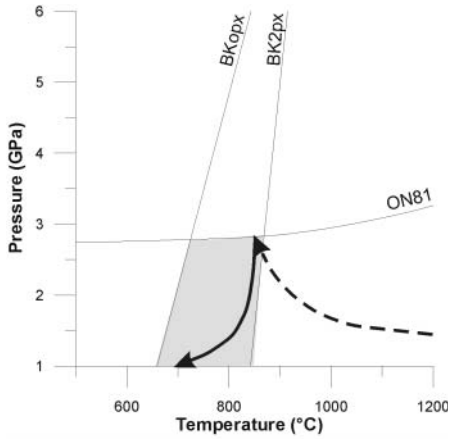

FIGURE 3. Geothermobarometry of the dissakisite-bearing type-sample A4310. ON81: spl-grt transition barometer of O'Neill (1981); BKcpx-opx and BKopx: two-pyroxene and Ca-in-Opx thermometers of Brey and Köhler (1990). The shaded field indicates the possible *P-T* field of formation of dissakisite-(La). The estimated *P-T* path of Ulten peridotites is shown for reference (thick solid line: retrograde path, after Godard et al. 1996; dashed line: prograde path, after Nimis and Morten 2000).

0.34–0.56; Al/(Al + Cr) = 0.45–0.70] is a common accessory phase. Pentlandite and copper sulfide minerals occur in minor amounts.

The spinel-amphibole-bearing paragenesis is interpreted to have developed after the eclogite-facies peak of subduction metamorphism at lower *P*, but higher P_{H_2O} (amphibolite/greenschist facies). The peak metamorphic pressure is estimated to be ≤2.7 GPa based on the spinel-garnet transition (O'Neill 1981; Fig. 3). Temperatures calculated with the two-pyroxene geothermometer of Brey and Köhler (1990) are within errors of peak temperatures of high-pressure metamorphism estimated for the Ulten peridotites by Nimis and Morten (2000) (c. 850 °C; Fig. 3). Temperatures calculated using the Ca-in-opx geothermometer of Brey and Köhler (1990) are about 100 °C lower. The former geothermometer is mostly dependent on the composition of the clinopyroxene, whereas the latter is based on the composition of orthopyroxene alone. The observed discrepancy may reflect either a faster reequilibration of orthopyroxene during retrogression or the large uncertainties of pyroxene geothermometry at temperatures below 800 °C. In any case, the thermobarometric data are consistent with formation of dissakisite-(La) either at the metamorphic pressure peak (eclogite-facies) or during subsequent retrogression.

Observations with a scanning electron microscope showed the common occurrence of mineral inclusions in the dissakisite-(La) crystals (Figs. 4a and 4b). The relative abundances of the included minerals were estimated by image analysis. In order of modal abundance, the identified minerals are (1) 47 vol% Mg-hornblende (X_{Mg} = 0.96); (2) 38 vol% chlorite (clinochlore X_{Mg} = 0.95); (3) 11 vol% (Th, U)-minerals [thorianite Th / (Th + U) [X_{Th}] = 0.64, uraninite X_{Th} = 0.08, minor thorite X_{Th} = 0.80]; and (4) 4 vol% Ca-minerals (calcite, apatite). Additional minor phases are Ba-rich phlogopite and dolomite. These inclusions account for 1.65 vol% of the bulk dissakisite crystal. The amphibole and chlorite,

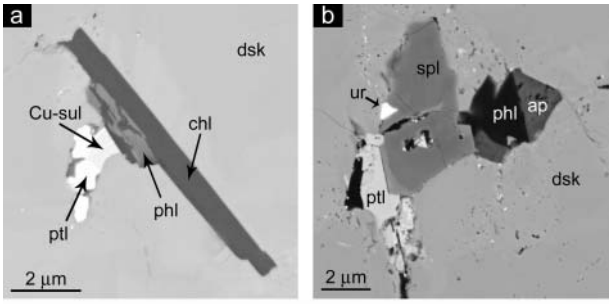

FIGURE 4. Backscattered-electron images of inclusions in dissakisite-(La) (dsk), type sample A4310; (**a**) chlorite (chl) with a relic of Ba-rich phlogopite (phl); (**b**) spinel (spl) and pentlandite (ptl). Other mineral abbreviations: uraninite (ur), apatite (ap), phlogopite (phl) and copper-rich sulfides (Cu-sul).

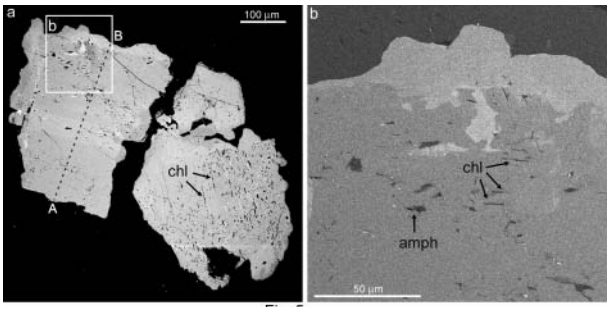

FIGURE 5. (**a**) Backscattered-electron image of dissakisite-(La) from sample A4310; (**b**) X-ray Th-U map of a detail of the strongly zoned rim. Abbreviations: chl = chlorite; amph = amphibole.

which occur as parallel lamellae in dissakisite (Fig. 5), probably developed by exsolution during retrogression, although an epitactic growth is not totally excluded. This suggests that dissakisite-(La) crystallized either at the eclogite-facies stage or during the early stage of retrogression. Crystallization under eclogite-facies conditions would be compatible with the experimentally determined stability field of allanite in the system KCMASH (up to 1150 °C and 4.5 GPa; Hermann 2002), and with the estimated metamorphic conditions for dissakisite-(Ce) from the Su-Lu terrane ($T \geq 760$ °C and $P \geq 4.2$ GPa; Yang and Jahn 2000).

PHYSICAL AND OPTICAL PROPERTIES

Macroscopically, dissakisite-(La) is translucent, black to very dark brown, becoming honey-brown in fragments thinner than 0.25 mm. The color of the powder (streak) is pale gray-greenish and the luster is pitch-like to vitreous. The Mohs hardness is 6.5–7. The mineral is brittle with a conchoidal fracture. The cleavage is imperfect on (001). The density, 3.79(15) g/cm^3, was measured using a Westphal balance and a grain of the type series (analysis carried out by G. Lucchetti). The calculated density of the DISS single crystal 5 is 3.84 g/cm^3.

The radioactivity is appreciable. Qualitative measurements using a SA-PHYMO-STEL SPP2-NF scintillometer gave 110 cps 5 cm from the detector and 150 cps at 0 cm (background 50–60 cps; estimated mass of the irradiating crystal c. 4 g).

Dissakisite-(La) is optically biaxial positive with α = 1.7395(25), β = 1.7434(25), γ = 1.7495(25) (589 nm light) (analysis carried out by G. Lucchetti). The maximum birefringence is 0.010. In 30 µm thin section it is pale brown with a greenish nuance and weakly pleochroic with X = light brown, $Y = Z$ green pale brown. $2V_{\gamma\,(meas.)}$ = 77.0(1)°, $2V_{\gamma\,(est.)}$ = 77.5°. Dispersion is medium with $r < v$. The optical orientation is $Y||\beta$; $X \wedge \gamma = 33(3)°$. Neither cathodoluminescence nor fluorescence was observed.

The yielded compatibility index (cf. Mandarino 1981; Bloss et al. 1983) is 1 – (K_p/K_C) = –0.013, i.e., excellent.

X-ray crystallography

Dissakisite-(La) is monoclinic, space group $P2_1/m$. Single-crystal diffractometer (Mo$K\alpha$) studies were carried out using sample DISS 3. Details of these studies will be described elsewhere (Lavina, Carbonin, Russo and Tumiati, unpublished manuscript).

Powder X-ray diffraction data (Table 1, Rietveld method using Cu$K\alpha$, λ = 1.5418; analysis performed by N. Masciocchi) were collected with a θ:θ Bruker AXS D8 diffractometer equipped with primary and secondary Soller slits (2.3°), divergence, antiscatter, and receiving slits (0.5°, 0.5°, and 0.2 mm, respectively), secondary beam curved graphite monochromator, Na(Tl)I scintillation detector, and pulse height amplifier discrimination. The generator was operated at 40 kV and 40 mA. The strongest observed lines were: [d(Å) (I)(hkl)] 2.926(100)(11$\bar{3}$), 2.860(53)(020), 2.553(51)(202), 3.526(49)(21$\bar{1}$), and 2.699(44)(120). The refined unit-cell parameters are a = 8.9616(7), b = 5.7265(5), and c = 10.2353(9) Å, β = 115.193(6)°, V = 475.30(7) Å^3, and Z = 2.

Raman spectroscopy

The spectrum of dissakisite-(La) (sample A4310) between 100 and 4000 cm^{-1} was collected using green (514 nm) laser radiation. The analysis was carried out with the collaboration of D. Smith and M.-C. Bernard. The most intense bands are at 958.9, 426.0, 455.2, 684.0, 1063.3, and 871.3 cm^{-1}. Less intense bands are at 565.8, 1184.4, 310.8, 226.4, 118.9 cm^{-1}. The band at 3067.6 cm^{-1} could represent the OH-stretching mode by similarity to that of zoisite (3151 cm^{-1}; Huang 1999). All the other bands between 1200 and 4000 cm^{-1} are attributed to the impregnating epoxy resin.

Chemical composition

Chemical analysis of dissakisite-(La) was performed by wavelength-dispersive electron microprobe analysis (EMPA) with a Cameca SX50 instrument at the University of Paris and by secondary ion mass spectrometry (SIMS) with a Cameca IMS4F instrument at the University of Montpellier II (see Appendix 1 for analytical procedures).

The empirical formula of dissakisite-(La) was calculated on the basis of 12.5 equivalent oxygen atoms and eight cations (Table 2). Estimation of the Fe^{3+}/Fe_{tot} ratio for charge balance yielded results that are consistent with the Mössbauer analysis performed at the University of Padova, which indicated that ferrous iron accounts for two thirds of the total iron (Lavina, Carbonin, Russo and Tumiati, unpublished manuscript). The H_2O content was calculated by stoichiometry assuming (OH) = 1, as for epidote-group minerals in general. Fluorine is believed to substitute for O in a combined substitution mechanism (Liebscher and Franz 2004). The final average formula of the type sample DISS 5 is: $(Ca_{1.195}Mn^*_{0.009}Sr^*_{0.010}Na_{0.002}Th_{0.090}U^*_{0.003}La_{0.315}Ce_{0.262}Pr^*_{0.019}Nd^*_{0.038}Sm^*_{0.002}Gd^*_{0.001}Er^*_{0.001})(Al_{1.816}Mg_{0.622}Fe^{2+}_{0.244}Fe^{3+}_{0.159}Cr_{0.148}Ti_{0.030}Sc^*_{0.002}V^*_{0.008}Ga^*_{0.001}Ni^*_{0.010}Zn^*_{0.015})(Si_{2.970}Al_{0.022}P^*_{0.008})O_{11.991}F_{0.009}(OH)$ (*SIMS analyses; Table 3). The La / (La + Ce) ratio is 0.545(16) for the type analysis (30 analyses) and 0.543(18) for sample A4310 (70 analyses) (cf. Fig. 6). Ce ≥ La has not been observed in any analysis. The name dissakisite-(La) was adopted according to the Levinson rules for the naming of REE minerals (Levinson 1966) and the definition of the species dissakisite-(Ce) given by Grew et al. (1991). The formula of dissakisite was initially calculated considering all included phases as exsolutions (1.65 vol%). The recalculated composition is not appreciably different from the measured composition, except for a slightly higher Mg content (Table 4).

Based on structural refinement, the simplified formula of the studied dissakisite can be expressed as (Ca, Fe^{2+}, Th, La)(La, REE, Ca)(Al, Cr, Ti)$_2$(Mg, Fe, Al)Si_3O_{12}(OH) (Lavina, Carbonin, Russo and Tumiati, unpublished manuscript). Characteristic of the Ulten dissakisite-(La) are the high Th contents (the highest so far reported for dissakisite) and Cr (cf. Yang and Enami 2003). Accordingly, the mineral should be described as a chromian, thorian, and cerian variety of dissakisite-(La).

The relations between major elements in dissakisite-(La) were investigated by principal component analysis (Fig. 7) and correlation matrix study (Table 5), using 54 chemical analyses representing a traverse of the large, zoned crystal of sample A4310 (Fig. 5). The first principal component (relative eigenvalue: 32.3%) reflects the weak zonation of the central part of the crystal, characterized by rimward increasing Fe, Ca, Al and decreasing Cr, Mg and Ti (Fig. 6). This trend could be the result of substitutions $REE^{3+} + Mg^{2+} \rightarrow Ca^{2+} + Fe^{3+}$ and $REE^{3+} + Mg^{2+} \rightarrow Ca^{2+} + Al^{3+}$, which relate dissakisite to epidote and clinozoisite (Gieré and Sorensen 2004, and references therein). The second principal component (rel. eigenvalue: 19.5%) shows a strong negative correlation between Th and the principal rare earth

TABLE 1. X–ray powder diffraction data for dissakisite–(La)

I/I_{obs}	d_{meas}	d_{calc}	$h\,k\,l$	I/I_{obs}	d_{meas}	d_{calc}	$h\,k\,l$
21	9.3	9.3	0 0 1	21	1.896	1.895	1 2 $\bar{4}$
13	8.1	8.1	1 0 0			1.894	2 2 $\bar{4}$
23	5.10	5.12	1 0 1			1.893	4 1 $\bar{4}$
29	4.86	4.87	0 1 1			1.888	1 1 $\bar{5}$
		4.68	1 1 0	15	1.882	1.883	3 1 2
24	4.67	4.66	1 1 $\bar{1}$			1.870	0 3 1
17	4.62	4.63	0 0 2			1.861	3 1 $\bar{5}$
15	4.05	4.05	2 0 0			1.858	1 3 0
14	4.00	4.01	2 0 $\bar{2}$	10	1.856	1.857	1 3 $\bar{1}$
11	3.80	3.82	1 1 1			1.852	0 0 5
		3.79	1 1 $\bar{2}$			1.802	4 0 $\bar{5}$
		3.60	0 1 2	10	1.800	1.800	0 2 4
49	3.53	3.53	2 1 $\bar{1}$			1.798	3 2 $\bar{4}$
11	3.44	3.44	1 0 2			1.788	1 3 1
		3.41	1 0–3			1.786	5 0 $\bar{2}$
		3.31	2 1 0	11	1.785	1.786	1 3 $\bar{2}$
17	3.28	3.29	2 1 $\bar{2}$			1.782	5 0 $\bar{3}$
27	3.24	3.24	2 0 1			1.765	0 3 2
12	3.19	3.20	2 0 $\bar{3}$			1.764	4 2 $\bar{2}$
11	3.12	3.09	0 0 3	10	1.762	1.762	0 1 5
		2.949	1 1 2	10	1.753	1.756	2 3 $\bar{1}$
		2.943	3 0 $\bar{2}$			1.739	4 1 1
100	2.926	2.928	1 1 $\bar{3}$	9	1.735	1.737	4 2 $\bar{1}$
53	2.860	2.863	0 2 0			1.727	5 0 $\bar{1}$
31	2.818	2.821	2 1 1			1.727	2 3 0
		2.793	2 1 $\bar{3}$			1.724	2 3 $\bar{2}$
41	2.714	2.717	0 1 3			1.720	2 0 4
		2.703	3 0 0	14	1.719	1.719	4 1 $\bar{5}$
44	2.699	2.700	1 2 0			1.715	5 0 $\bar{4}$
		2.697	1 2 $\bar{1}$			1.705	3 0 3
18	2.671	2.675	3 0 $\bar{3}$			1.705	5 1 $\bar{2}$
38	2.623	2.626	3 1 $\bar{1}$	12	1.704	1.704	2 0 $\bar{6}$
		2.617	3 1 $\bar{2}$			1.701	5 1 $\bar{3}$
51	2.553	2.558	2 0 2			1.684	3 0 $\bar{6}$
		2.529	1 0 $\bar{4}$			1.677	2 2 3
17	2.526	2.526	2 0 $\bar{4}$			1.669	1 3 2
		2.499	1 2 1			1.665	1 3 $\bar{3}$
18	2.491	2.491	1 2 $\bar{2}$	19	1.664	1.665	2 2 $\bar{5}$
		2.435	0 2 2			1.659	1 0 5
19	2.424	2.423	3 1 $\bar{3}$			1.655	4 2 0
		2.413	2 2 $\bar{1}$			1.654	5 1 $\bar{1}$
		2.336	2 1 2	25	1.651	1.651	1 0 $\bar{6}$
		2.331	2 2 $\bar{2}$			1.647	2 1 4
17	2.328	2.327	1 1 3			1.646	1 2 4
		2.315	0 0 4	25	1.644	1.645	2 3 1
14	2.312	2.313	1 1 $\bar{4}$			1.643	4 2 $\bar{4}$
		2.311	2 1 $\bar{4}$			1.643	5 1 $\bar{4}$
		2.310	3 0 $\bar{4}$			1.640	1 2 $\bar{5}$
		2.240	4 0 $\bar{2}$			1.639	2 3 $\bar{3}$
		2.192	1 2 $\bar{3}$			1.636	3 2 2
24	2.184	2.184	4 0 $\bar{1}$			1.635	3 1 3
		2.171	4 0 $\bar{3}$			1.633	2 1 $\bar{6}$
		2.167	3 1 1	13	1.623	1.624	0 3 3
		2.147	0 1 4			1.622	5 0 0
26	2.144	2.146	2 2 1			1.622	3 2 $\bar{5}$
		2.142	3 1 $\bar{4}$			1.621	4 0 2
24	2.132	2.133	2 2 $\bar{3}$			1.616	3 1 $\bar{6}$
16	2.099	2.099	0 2 3			1.605	5 0 $\bar{5}$
		2.086	4 1 $\bar{2}$			1.603	3 3 $\bar{1}$
21	2.067	2.068	2 0 3	23	1.600	1.601	3 3 $\bar{2}$
		2.056	3 2 $\bar{1}$			1.599	4 0 $\bar{6}$
		2.052	3 2 $\bar{2}$	18	1.595	1.593	1 1 5
		2.046	2 0 $\bar{5}$			1.586	1 1 $\bar{6}$
		2.041	4 1 $\bar{1}$			1.560	5 1 0
		2.030	4 1 $\bar{3}$			1.560	4 1 2
11	2.028	2.027	4 0 0			1.559	3 3 0
		2.012	1 0 4	13	1.556	1.555	0 2 5
		2.006	4 0 $\bar{4}$			1.554	3 3 $\bar{3}$
		1.968	3 0 $\bar{5}$				
10	1.946	1.945	2 1 3				
		1.911	4 1 0				
16	1.906	1.908	2 2 2				
		1.903	1 2 3				
		1.898	1 1 4				

elements (La, Ce, Nd), which corresponds to a zonation restricted to the outer rim of the crystal (Fig. 5b). This correlation suggests a substitution mechanism similar to that proposed for monazite, i.e., $Th^{4+} + Ca^{2+} \rightarrow 2REE^{3+}$.

As a general feature, dissakisite-(La) is rich in trace elements (Table 3 and 4). Chondrite-normalized REE concentrations show a regular decrease from La to Lu, interrupted by an Er-Tm peak (Fig. 8). An enrichment in Er (183 ppm) has also been reported by Sassi et al. (2000) for the allanitic core of an epidote occurring in a qtz + grt ± coe eclogite from Dabieshan (China).

Isotopic data

Sm-Nd isotope analysis of c. 0.5 mg of an optically clean, hand-picked concentrate of dissakisite-(La) (Table 6) was performed at the Laboratory for Geochronology of the Vienna University-Geozentrum with the collaboration of M. Thöni (for the analytical methods see Tumiati et al. 2003). The Sm/Nd ratio is extremely low (0.045), consistent with the strong Light Rare Earths Element (LREE) fractionation of allanites. Despite the overall LREE enrichment, the positive ε(t) value of +1.7 (recalculated for t = 330 Ma; see below) indicates a depletion in non-radiogenic Nd.

Discussion

The first occurrence of dissakisite in peridotite concerned a 0.22 mm sized relic of chromian dissakisite-(Ce) included in a clinopyroxene of the garnet-bearing peridotite of Zhimafang, Su-Lu ultra-high-pressure metamorphic terrane, eastern China (Yang and Enami 2003). Formation of dissakisite-(Ce) is believed to have predated recrystallization of the host peridotite, which occurred at 760 °C and 4.2 GPa (Yang and Jahn 2000). The dissakisite-(La) from the Ulten zone reported in the present study occurs as up to centimeter-sized crystals in the olivine matrix of a retrogressed spinel-amphibole peridotite. Based on petrographic evidence and thermobarometric estimates, the Ulten dissakisite-(La) formed at $P \leq 2.7$ GPa and $T \leq 850$ °C. In both cases the dissakisite-bearing peridotites are hosted by high-pressure gneisses (cf. for Ulten, e.g., Godard et al. 1996; for Su-Lu, e.g., Medaris 1999). A high- or ultra-high-pressure genesis of peridotite-hosted dissakisite is compatible with the recent experimental results of Hermann (2002), who found a negative-slope for the allanite-in/zoisite-out curve starting at T = 850 °C and P = 2.0 GPa, and ending at T = 710 °C and P = 3.5 GPa. In fact, as the author worked in a REE-doped KCMASH

Table 2. Chemical analysis of dissakisite-(La) and chemical formula calculated on the basis of 8 cations, 1 (OH), and 12 (F + O)

Oxides	wt%	Elements	afu
SiO_2*	32.41	Si	2.970
P_2O_5†	0.10	P	0.008
ThO_2*	4.29	Th	0.090
UO_2†	0.14	U	0.003
TiO_2*	0.44	Ti	0.030
Al_2O_3*	17.02	Al	1.838
Cr_2O_3*	2.05	Cr	0.148
Sc_2O_3†	0.02	Sc	0.002
V_2O_3†	0.11	V	0.008
Ga_2O_3†	0.02	Ga	0.001
La_2O_3*	9.31	La	0.315
Ce_2O_3*	7.83	Ce	0.262
Pr_2O_3†	0.56	Pr	0.019
Nd_2O_3†	1.15	Nd	0.038
Sm_2O_3†	0.06	Sm	0.002
Gd_2O_3†	0.03	Gd	0.001
Er_2O_3†	0.05	Er	0.001
FeO*	3.19	Fe^{2+}	0.244
Fe_2O_3‡	2.31	Fe^{3+}	0.159
CaO*	12.18	Ca	1.195
MnO†	0.11	Mn	0.009
MgO*	4.55	Mg	0.622
SrO†	0.18	Sr	0.010
NiO†	0.14	Ni	0.010
ZnO†	0.22	Zn	0.015
Na_2O*	0.01	Na	0.002
F*	0.03	$\Sigma_{cations}$	8.000
H_2O‡	1.62		
–O = F	–0.01	OH	1.000
Total	100.11	F	0.009
		O	11.991
Fe^{2+}/Fe_{tot}	0.61		
La/La + Ce	0.545		

* Analyzed by EMPA.
† Analyzed by SIMS.
‡ Calculated by stoichiometry.

Table 3. SIMS analysis of dissakisite-(La) obtained using the energy filtering method

	Mean values (ppm)	±2σ	Detection limit (ppm)
P	415	105	37.2
Sc	127	17.7	3.93
V	775	74.8	16.9
Mn	840	64.4	19.5
Co	50.0	2.17	3.70
Ni	1078	89.6	32.6
Cu	29.1	12.7	11.2
Zn	1738	259	176
Ga	114	4.63	17.1
Ge	1.89	0.34	0.43
Rb	3.38	1.08	0.64
Sr	1535	390	23.4
Y	38.4	25.6	3.33
Zr	32.3	20.4	2.08
Nb	0.54	0.12	0.19
Cs	0.13	0.49	0.08
Ba	54.9	34.3	10.9
U	1222	642	47.5
Pr	4851	52.5	61.1
Nd	9829	169	241
Sm	512	3.63	48.6
Eu	74.9	2.31	10.5
Gd*	182	91	9.21
Tb*	14	7	1.35
Dy	44.8	1.82	12.0
Ho	3.16	0.61	1.03
Er	364	17.1	37.6
Tm	8.22	0.54	1.22
Yb*	n. d.	–	8
Lu*	n. d.	–	1

Note: n.d. = not detected.
*Analyzed using the high-resolution method.

Table 4. EMPA chemical composition of the main mineral inclusions

	Included minerals				Dissakisite	
	Thorianite	Chlorite	Amphibole	Calcite	Final	Initial
K			0.020			0.000
Na			0.200			0.001
Mg		4.470	4.360	0.030	0.710	0.732
Al		2.070	0.900		1.910	1.900
Si		3.010	7.410		3.000	3.002
Fe		0.220	0.260		0.380	0.378
Mn			0.010			0.000
U	0.350					0.003
Th	0.630				0.090	0.094
Ce					0.260	0.257
La					0.290	0.287
Gd					0.020	0.020
Pr					0.010	0.010
Ti		0.010	0.020		0.030	0.030
F		0.030			0.010	0.010
Cr		0.120	0.080		0.120	0.119
Ca		0.010	1.940	0.970	1.170	1.166
Pb	0.020					0.000
C				1.000		0.002
OH		7.970	2.000		1.000	1.000
O	2.000	10.000	22.000	3.000	11.990	11.990

Note: Measured final and estimated initial dissakisite-(La) compositions are shown for comparison.

Table 5. Correlation matrix for the dissakisite-(La) EMPA data (cf. Fig. 6)

Ti	1										
Th	**–0.389**	1									
Al	**–0.717**	0.136	1								
Cr	**0.472**	0.077	**–0.721**	1							
Fe	**–0.606**	0.173	**0.399**	**–0.427**	1						
La	0.134	**–0.310**	–0.032	–0.160	–0.079	1					
Ce	**0.542**	**–0.685**	**–0.319**	0.020	–0.223	0.156	1				
Pr	0.081	–0.076	–0.161	0.048	–0.011	0.061	–0.018	1			
Nd	**0.273**	**–0.495**	–0.115	0.035	–0.174	0.036	**0.332**	0.109	1		
Ca	**–0.648**	0.229	**0.525**	**–0.466**	**0.617**	–0.087	–0.176	–0.076	–0.165	1	
Mg	**0.645**	–0.136	**–0.657**	**0.606**	**–0.665**	–0.093	0.124	–0.011	0.072	**–0.897**	1
	Ti	Th	Al	Cr	Fe	La	Ce	Pr	Nd	Ca	Mg

Note: Significant values ($\alpha = 0.050$, two-tailed test), except diagonal, are printed in bold.

Table 6. Sm–Nd isotope data of dissakisite-(La)

Sample no./locality	Sm (ppm)	Nd (ppm)	$^{147}Sm/^{144}Nd$	$^{143}Nd/^{144}Nd$	$\pm 2\sigma_m$	$\varepsilon_{Nd}(330)$
A4310/Hochwart	340.917	7629.115	0.0270	0.512357	5.50E-06	+1.7

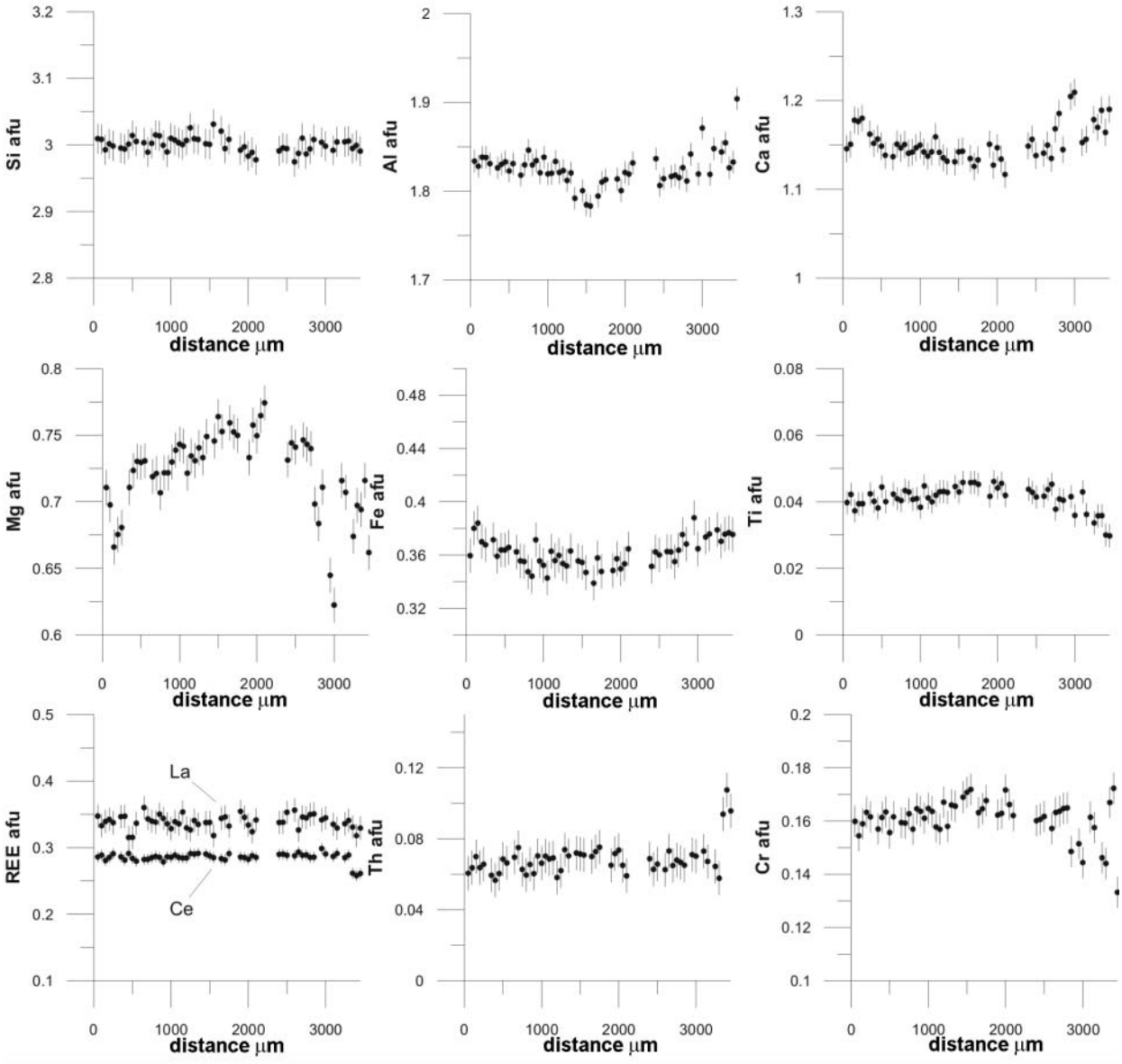

Figure 6. Microprobe traverse of sample A4310 (A-B in Fig. 5). The vertical bars represent ±2σ uncertainties (see Appendix 1).

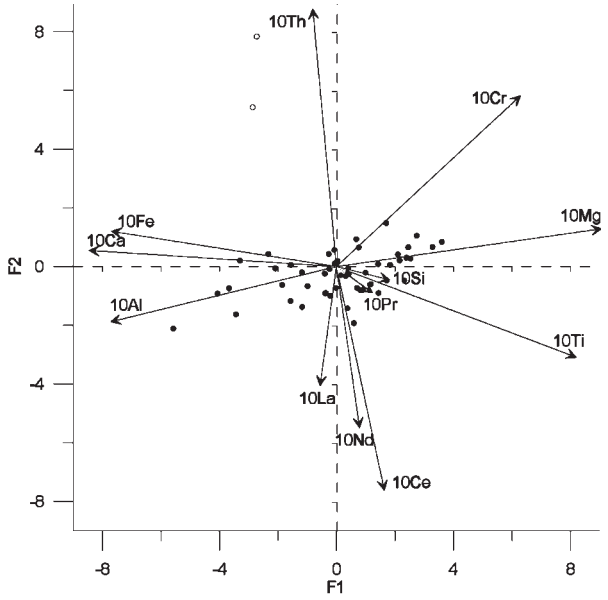

FIGURE 7. Principal component analysis of EMPA data of dissakisite-(La) (cf. Fig. 6). Empty symbols refer to the outer rim of the crystal. Arrows represent 10 moles of an element expressed as a linear combination of the two main principal components F1 and F2.

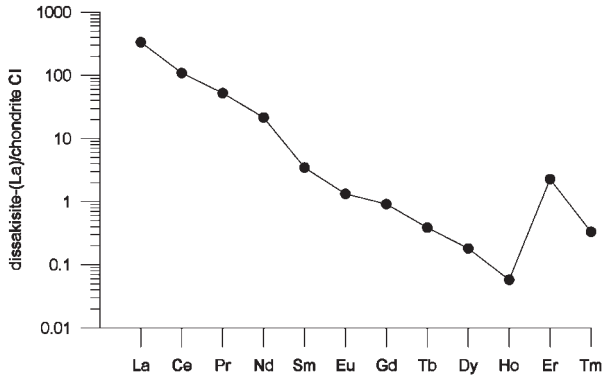

FIGURE 8. Chondrite-normalized REE data for dissakisite-(La). Normalizing values were taken from McDonough and Sun (1995).

system, his "allanite" is actually dissakisite.

Whereas Su-Lu peridotite-bearing gneisses do not display evidence of partial melting (Yang, pers. comm.), migmatization is widespread in the Ulten gneisses (Godard et al. 1996; Martin et al. 1998; Del Moro et al. 1999). This process is believed to have played an important role in the LILE (i.e., LREE, Sr, Ba, Rb) metasomatism of the entrained peridotites (Rampone and Morten 2001; Tumiati et al. 2003). Hauzenberger et al. (1996) proposed that migmatization of the Ulten gneisses occurred by prograde, fluid-saturated, partial melting. The general absence of white mica and abundance of garnet + kyanite in the restitic assemblages suggest that the gneisses passed through a muscovite (phengite)-dehydration melting reaction along either a prograde or decompressional path (Tumiati et al. 2003). During crystallization of the melt, a water-rich fluid phase was released, as testified by H_2O-rich fluid inclusions in the quartz of the leucosomes of the migmatitic gneisses (Höller and Hoinkes 1996). According to Rampone and Morten (2001), reactions between the peridotites and a LILE-enriched, High-Field-Strength Elements (HFSE)-depleted metasomatizing fluid with a low CO_2/H_2O ratio were responsible for the LREE and Sr enrichment in clinopyroxene, and the crystallization of abundant LILE-rich, HFSE-poor, pargasitic amphibole. Using isotopic data, Tumiati et al. (2003) found the same Sm-Nd ages for the migmatization and the H*P* metamorphism of Ulten gneisses. They also provided evidence for the concurrent introduction of crustal Nd in the amphibole-bearing garnet peridotites, thus supporting the strict link between gneiss migmatization and peridotite metasomatism.

Data on partitioning of REE between allanite and aqueous fluid indicate strongly compatible behavior of LREE, but a relatively flat LREE pattern (Banks et al. 1994; Frei et al. 2004). In particular, Banks et al. (1994) found similar values of $D_{La}^{aln/fluid}$ and $D_{Ce}^{aln/fluid}$. Therefore the high La/(La + Ce) ratio of our dissakisite-(La) would require crystallization from a fluid characterized by La > Ce. Such a fluid could be the result of several processes, such as: (1) fractionation of garnet with Ce > La in the restite during migmatization, (2) La/Ce fractionation during fluid release from the melt (cf. Flynn and Burnham 1978), and (3) La/Ce fractionation during amphibole formation in the peridotite.

ACKNOWLEDGMENTS

The authors are indebted to M. Thöni (University of Vienna), G. Lucchetti (University of Genova), N. Masciocchi (University of Insubria), P. Frizzo (University of Padova), R. Carampin (CNR-Padova), M. Fialin, D. Smith, M.-C. Bernard, and A. Hugot-Le Goff (CNRS-Paris) for access to the analytical facilities. Reviews by S. Poli, G. Franz, and J. Ayers substantially contributed to improving the manuscript. S.T. was supported during the study by a fellowship of the "Fondazione Ing. Aldo Gini" (Padova). Financial support of the Provincia Autonoma di Bolzano—Autonome Provinz Bozen and the Provincia Automona di Trento (CARG-PAT), Italian MIUR ex-60% grants and CNR-IGG (Padova) is gratefully acknowledged.

REFERENCES CITED

Andreatta, C. (1936) La formazione gneissico-kinzigitica e le oliviniti di Val d'Ultimo (Alto Adige). Memorie del Museo di Storia Naturale della Venezia Tridentina, 3, 87–245.

Banks, D.A., Yardley, B.W.D., Campbell, A.R., and Jarvis, K.E. (1994) REE composition of an aqueous magmatic fluid: A fluid inclusion study from the Capitan Pluton, New Mexico, U.S.A. Chemical Geology, 113, 259–272.

Bloss, F.D., Gunter, M., Shu-Chun, S., and Wolfe, H.E. (1983) Gladstone-Dale constants; a new approach. Canadian Mineralogist, 21, 93–99.

Bondi, M., De Francesco, A.M., and Morten, L. (1992) Major elements, 3d transition elements, Cu and Sr geochemistry of peridotitic rocks within the Austridic crystalline basement, Nonsberg area, Northern Italy. International Geoscience Programme 276, Newsletter 5, 229–235.

Bottazzi, P., Ottolini, L., and Vannucci, R. (1992) SIMS analyses of rare earth elements in natural minerals and glasses: An investigation of structural matrix on ion yields. Scanning, 14, 160–168.

Brey, G.P. and Köhler, T. (1990) Geothermobarometry in four-phase lherzolites II. New thermobarometers, and practical assessment of existing thermobarometers. Journal of Petrology, 31-6, 1353–1378.

Del Moro, A., Martin, S., and Prosser, G. (1999) Migmatites of the Ulten zone (NE Italy), record of melt transfer in deep crust. Journal of Petrology, 40–12, 1803–1826.

Drake, M.J. and Weill, D.F. (1972) New rare earth element standards for electron microprobe analysis. Chemical Geology, 10, 179–181.

Enami, M. and Zang, Q. (1988) Magnesian staurolite in garnet-corundum rocks and eclogite from the Donghai district, Jiangsu Province, east China. American Mineralogist, 73, 48–56.

Ercit, T.S. (2002) The mess that is "allanite". Canadian Mineralogist, 40, 1411–1419.

Fahey, A.J. (1998) Details of the measurements of rare earth and other trace element abundances by secondary ion mass spectrometry. International Journal of Mass Spectrometry, 176, 63–76.

Flynn, R.T. and Burnham, C.W. (1978) An experimental determination of rare earth

partition coefficients between a chloride containing vapor phase and silicate melts. Geochimica et Cosmochimica Acta, 42, 685–701.
Frei, D., Liebscher, A., Franz, G., and Dulski, P. (2004) Trace element geochemistry of epidote minerals. In A. Liebscher and G. Franz, Eds., Epidotes, 56, 553–605. Reviews in Mineralogy and Geochemistry, Mineralogical Society of America, Washington, D.C.
Geijer, P. (1927) Some mineral associations from the Norberg District. Sveriges Geologiska Undersokning. Avhandlingar och uppsatser series C 343 (Arsbok 20, 1926, No.4), 1–32.
Gieré, R. and Sorensen, S. S. (2004) Allanite and other REE-rich epidote-group minerals. In A. Liebscher and G. Franz, Eds., Epidotes, 56, 431–493. Reviews in Mineralogy and Geochemistry, Mineralogical Society of America, Washington, D.C.
Godard, G. and Martin, S. (2000) Petrogenesis of kelyphites in garnet peridotites: a case study from the Ulten zone, Italian Alps. Journal of Geodynamics, 30, 117–145.
Godard, G., Martin, S., Prosser, G., Kienast, J.R., and Morten, L. (1996) Variscan migmatites, eclogites and garnet-peridotites of the Ulten zone, Eastern Austroalpine system. Tectonophysics, 259, 313–341.
Grew, E.S., Essene, E.J., Peacor, D.R., Su, S.C., and Asami, M. (1991) Dissakisite-(Ce), a new member of the epidote group and the Mg analogue of allanite-(Ce), from Antarctica. American Mineralogist, 76, 1990–1997.
Hauzenberger, C.A., Höller, W., and Hoinkes, G. (1996) Transition from eclogite to amphibolite-facies metamorphism in the austroalpine Ulten zone. Mineralogy and Petrology, 56, 111–130.
Hermann, J. (2002) Allanite; thorium and light rare earth element carrier in subducted crust. Chemical Geology, 192, 289–306.
Höller, W. and Hoinkes, G. (1996) Fluid evolution during high-pressure partial melting in the austroalpine Ulten zone, northern Italy. Mineralogy and Petrology, 58, 131–144.
Huang, E. (1999) Raman spectroscopic study of 15 gem minerals. Journal of the Geological Society of China, 42, 301–318.
Khvostova, V.A. and Bykova, A.V. (1961) Accessory orthite of southern Yakutia. Institut mineralogii, geokhimii I kristallokhimii redkikh elementov Akademii nauk SSSR, Trudy, 7, 130–137.
Levinson, A.A. (1966) A system of nomenclature for rare-earth minerals. American Mineralogist, 51, 152–158.
Liebscher, A. and Franz, G., Eds. (2004) Epidotes. Reviews in Mineralogy and Geochemistry, Mineralogical Society of America, Washington, D.C.
Mandarino, J.A. (1981) The Gladstone-Dale relationship; Part IV, The compatibility concept and its application. Canadian Mineralogist, 19, 441–450.
Martin, S., Godard, G., Prosser, G., Schiavo, A., Bernoulli, D., and Ranalli, G. (1998) Evolution of the deep crust at the junction Austoalpine/Southalpine: the Tonale nappe. Memorie di Scienze Geologiche dell'Università di Padova, 50, 3–50.
McDonough, W.F. and Sun, S.-s. (1995) The composition of the Earth. Chemical Geology, 120, 223–253.
Medaris, L.G. (1999) Garnet peridotites in Eurasian high-pressure and ultrahigh-pressure terranes: a diversity of origins and thermal histories. International Geology Review, 41, 799–815.
Moëlo, Y., Choutier, J.P., and Gilles, C. (1974) Minéralogie de la France: Allanite. Bulletin de la Société Française de Minéralogie et Cristallographie, 97, 521.
Morten, L. and Obata, M. (1990) Rare earth abundances in the eastern Alpine peridotites, Nonsberg area, Northern Italy. European Journal of Mineralogy, 2, 643–653.
Nimis, P. and Morten, L. (2000) *P-T* evolution of 'crustal' garnet peridotites and included pyroxenites from Nonsberg area (upper Austroalpine), NE Italy: from the wedge to the slab. Journal of Geodynamics, 30, 93–115.
Ntaflos, T., Thöni, M., und Yin, Q. (1993) Geochemie der Ultentaler Ultramafitite. Mitteilungen der Österreichischen und Mineralogischen Gesellschaft, 138, 169–178.
Obata, M. and Morten, L. (1987) Transformation of spinel lherzolite to garnet lherzolite in ultramafic lenses of the austridic crystalline complex, northern Italy. Journal of Petrology, 28–3, 599–623.
O'Neill, H.St.C. (1981) The transition between spinel lherzolite and garnet lherzolite, and its use as a geobarometer. Contributions to Mineralogy and Petrology, 77, 185–194.
Parseval, P. de, Fontan, F., and Aigouy, T. (1997) Chemical composition of REE minerals from Trimouns (French Pyrenees). Comptes-Rendus hebdomadaires de l'Académie des Sciences de Paris, 324, 625–630.
Petrini, R. and Morten, L. (1993) Nd-isotopic evidence of enriched lithospheric domains: An example from the Nonsberg Area, Eastern Alps. Terra Abstracts, 5, 19–20.
Rampone, E. and Morten, L. (2001) Records of crustal metasomatism in the garnet peridotites of the Ulten Zone (Upper Austroalpine, Eastern Alps). Journal of Petrology, 42, 207–219.
Rocholl, A.B.E., Simon, K., Jochum, K.P., Bruhn, F., Gehann, R., Kramar, U., Luecke, W., Molzahn, M., Pernicka, E., Seufert, M., Spettel, B., and Stummeier, J. (1997) Chemical characterisation of NIST silicate glass certified reference material SRM 6 10 by ICP-MS, TIMS, LIMS, SSMS, INAA, AAS and PIXE. Geostandards Newsletter: The Journal of Geostandards and Geoanalysis, 21, 101–114.
Rost, F. und Brenneis, P. (1978) Die Ultramafitite im Bergzug südlich des Ultentales, Provinz Alto Adige (Oberitalien). Tschermaks Mineralogiche und Petrographische Mitteilungen, 25, 257–286.
Sassi, R., Harte, B., Carswell, D.A., and Yujing, H. (2000) Trace element distribution in Central Dabie eclogites. Contributions to Mineralogy and Petrology, 139, 298–315.
Shimizu, H., Semet, M., and Allegre, C.J. (1978) Geochemical application of quantitative ion-microprobe analysis. Geochimica et Cosmochimica Acta, 42, 1321–1334.
Susini, S. e Martin, S. (1996) Microstrutture nelle peridotiti della Serie d'Ultimo (Austroalpino Superiore, Alpi Orientali). Atti Ticinesi di Scienze della Terra, Serie speciale, 4, 47–63.
Treloar, P.J. and Charnley, N.R. (1987) Chromian allanite from Outokumpu, Finland. Canadian Mineralogist, 25, 413–418.
Tumiati, S. and Martin, S. (2003) Garnet-peridotite in the Italian Eastern Alps: 150 years of discoveries. Memorie di Scienze Geologiche dell'Università di Padova, 55, 31–46.
Tumiati, S., Thöni, M., Nimis, P., Martin, S., and Mair, V. (2003) Mantle-crust interactions during Variscan subduction in the Eastern Alps (Nonsberg-Ulten Zone): geochronology and new petrological constraints. Earth and Planetary Science Letters, 210, 509–526.
Yang, J.J. and Enami, M. (2003) Chromian dissakisite-(Ce) in a garnet lherzolite from the Chinese Su-Lu UHP metamorphic terrane: Implications for Cr incorporation in epidote-group minerals and recycling of REE into the Earth's mantle. American Mineralogist, 88, 604–610.
Yang, J.J. and Jahn, B.M. (2000) Deep subduction of mantle-derived garnet lherzolites from the Su-Lu UHP metamorphic terrane in China. Journal of Metamorphic Geology, 18, 167–180.
Zakrzewski, M.A., Lustenhouwer, W.J., Nugteren, H.J., and Williams, C.T. (1992) Rare-earth minerals yttrian zirconolite and allanite-(Ce) and associated minerals from Koberg mine, Bergslagen, Sweden. Mineralogical Magazine, 56, 27–35.
Zinner, E. and Crozaz, G. (1986) A method for quantitative measurement of rare earth elements in the ion microprobe. International Journal of Mass Spectrometry and Ion Processes, 69, 17–38.

MANUSCRIPT RECEIVED MAY 13, 2004
MANUSCRIPT ACCEPTED NOVEMBER 25, 2004
MANUSCRIPT HANDLED BY JOHN AYERS

APPENDIX 1

Chemical analysis of dissakisite-(La) was performed using the Cameca SX50 wavelength-dispersive electron microprobe (EMPA) at the University of Paris and by secondary ion mass spectrometry (SIMS) with a Cameca IMS4F instrument at the University of Montpellier II. Samples and standards were polished to provide a flat surface for sputtering of secondary ions. The surfaces of the samples were carbon-coated to prevent charging.

Operating conditions for EMP analysis were a 15 kV accelerating potential, a 40 nA sample current, and a 1 μm beam diameter. The following pure minerals and synthetic materials were used as standards: diopside (for Ca, Mg and Si), Fe_2O_3 (for Fe), orthoclase (for Al), Cr_2O_3 (for Cr), La_3ReO_8 (for La), monazite (for Ce and Th), REE glass (for Pr), Cu-Nd alloy (for Nd), and $MnTiO_3$ (for Ti). A counting time of 10 s was used for all elements. Estimation of the analytical precision was performed by analyzing the same point 30 times. Relative errors were <1% for Ca, Mg, Al, and Si; <2% for Fe and Ce; <3% for Cr and La; and <6% for Ti and Th. Relative errors for Nd and Pr were very high (20% and 45% respectively). Therefore, these elements were further analyzed by SIMS (<2% rel.; Tables 3 and 4).

Spots for SIMS microanalysis were selected after detailed petrographic and electron probe analysis. Negative oxygen ions with an accelerating potential of 15 kV were used as primary

ions. A 20 nA O^- primary beam was focused to sputter a flat-bottomed crater (25 μm diameter) on the sample. Before collecting secondary ions, the surface was sputtered for five minutes to remove the carbon coating the spot. The surrounding carbon coat was sufficient to keep the surface from charging. Positive secondary ions for mass analysis were extracted with a 4.5 kV accelerating voltage. Secondary ions were detected by means of an electron multiplier operating in the ion counting mode. For the quantitative measurements of REEs, the energy filtering technique was adopted (Shimizu et al. 1978) using a 30 eV energy window, a high-energy offset of 80 eV, and fully open entrance and exit slits.

Each measurement consisted of a twelve-cycle routine, during which the magnet was cyclically peak-stepped through the masses. Two groups of masses were chosen to be measured from each spot: one consisted of 25.5 (for background), $^{30}Si^+$,$^{137}Ba^+$, $^{141}Pr^+$, $^{143}Nd^+$, $^{147}Sm^+$, $^{151}Eu^+$, $^{159}Tb^+$, $^{160}Gd^+$, $^{163}Dy^+$, $^{165}Ho^+$, $^{167}Er^+$, $^{169}Tm^+$, $^{174}Yb^+$, $^{175}Lu^+$, $^{178}Hf^+$, $^{181}Ta^+$, $^{184}W^+$, and $^{238}U^+$, the other of 25.5 (background), $^{30}Si^+$, $^{49}Ti^+$, $^{51}V^+$, $^{55}Mn^+$, $^{63}Cu^+$, $^{69}Ga^+$, $^{74}Ge^+$, $^{85}Rb^+$, $^{88}Sr^+$, $^{89}Y^+$, $^{90}Zr^+$, and $^{93}Nb^+$. The counting time for each peak varied from 2 s (from Si to Ge and for light REEs) to 10 s (heavy REEs) or 30 s (from Yb to U). Owing to their very high concentrations, La and Ce could not be measured because of saturation of the electron multiplier and their concentrations were determined by EPM analysis.

NIST SRM 610 silicate glasses were used, under the same analytical conditions, for calibration of all elements. The working values were those proposed by Rocholl et al. (1997). Since the Si concentration of the NIST 610 glass standard and that of dissakisite were known from electron microprobe analysis, $^{30}Si^+$ was used as an internal standard. The secondary ion yields of mass M were obtained by dividing $M^+/^{30}Si^+$ by the concentration of element of mass M in the standard. They were determined after correction for detector dead time (30 ns) and background (0.5 counts per minute). The precision of the yields is typically 5% at the 1σ level over one year on the NIST 610 standard. This precision, estimated by the reproducibility of $M^+/^{30}Si^+$ ratios, is larger than the error calculated by ion-counting statistics and takes into account standard charging and non-homogeneity, apparatus drift, detector efficiency, etc. The trend of the yield variation agrees well with that reported by various authors. The average of these secondary ion yields was used to determine the element concentration.

Although the energy-filtering technique reduces the effect of most molecular interferences, monoxides can produce significant interferences, and have to be corrected for. The intensity of an interfering oxide depend on the element concentration of the interfering oxide, its isotopic abundance, and the oxide-to-element ratios of the interfering species. In our study, some REE oxides produce significant interferences: $^{144}NdO+$ and $^{144}SmO^+$ with $^{160}Gd^+$, $^{143}NdO^+$ with $^{159}Tb^+$, $^{149}SmO^+$ with $^{165}Ho^+$, $^{151}EuO^+$ with $^{167}Er^+$, $^{158}GdO^+$ with $^{174}Yb^+$, $^{159}TbO^+$ with $^{175}Lu^+$, $^{162}DyO^+$ with $^{178}Hf^+$, and $^{168}ErO^+$ with $^{184}W^+$. To determine the oxide-to-element ratio to be used for the corrections, Drake and Weill (1972) REE glass standards were measured. Detailed descriptions of the data reduction procedure have been presented by several authors (Zinner and Crozaz 1986; Bottazzi et al. 1992; Fahey 1998). Owing to the high concentrations of Nd and Sm, their interferences with Gd and Tb were particularly severe. An evaluation of Tb and Gd was attempted using the High-Resolution (HR) method. Corrections for interferences contribute to an overall reduction of the precision of the data. Thus, an uncertainty of 10% was assumed for each oxide-to-element ratio. This is larger than the precision obtained on the Drake and Weill REE glass standards, and takes into account small differences between samples and standard resulting from matrix and charging effect. The increase of uncertainty is amplified for samples with high LREE/HREE ratios.